Eur. Phys. J. B **40**, 471–478 (2004)
DOI: 10.1140/epjb/e2004-00229-3

THE EUROPEAN PHYSICAL JOURNAL B

Vortex patterns and nucleation of superconductivity in mesoscopic rectangles and in hybrid superconductor/ferromagnet structures

V.V. Moshchalkov, M. Morelle[a], G. Teniers, and D.S. Golubović

Nanoscale Superconductivity and Magnetism Group, Laboratory for Solid State Physics and Magnetism, K.U. Leuven, Celestijnenlaan 200D, 3001 Leuven, Belgium

Received 26 February 2004
Published online 3 August 2004 –

Abstract. Nucleation of superconductivity and vortex patterns have been studied in mesoscopic samples providing the crossover between square and rectangular geometries. The measured nucleation line, $T_c(H)$, has been analyzed in the framework of the linearized Ginzburg-Landau theory. A very good agreement has been found between the theoretical $T_c(H)$ boundary and the experimental data for rectangles with different aspect ratios. The superconductor/ferromagnet hybrids, such as magnetic Co/Pd dot in a superconducting loop and the dot on top of a superconducting disk have also been investigated. Pronounced effects of the dot on the $T_c(H)$ boundary have been found, including strong asymmetry with respect to the field polarity.

PACS. 74.25.Dw Superconductivity phase diagrams – 74.78.Na Mesoscopic and nanoscale systems

1 Introduction

Superconductivity is a remarkable example of macroscopic quantum phenomena: the condensate of the Cooper pairs, even in large samples, is described by the complex order parameter $\Psi = |\Psi| e^{i\phi}$ obeying the Ginzburg-Landau (GL) equations. This is very much like in quantum systems where the wave function Ψ is obeying the Schrödinger equation. Interestingly, the linearized GL equation practically coincides with the Schrödinger equation without potential $U(\overrightarrow{r})$, provided that instead of the single electron charge e the charge $2e$ of the Cooper pair is used and also the eigenvalue E in the Schrödinger equation is replaced by the first GL parameter, $-\alpha$, here $-\alpha = \hbar^2/2m^*\xi^2(T)$ with $\xi(T)$ the temperature dependent coherence length.

The behavior of the superconducting condensate, confined by the sample boundaries, can be compared with a quantum-mechanical problem 'particle in a box'. By varying the size and the shape of the box, its quantum levels can be substantially modified. Along the same lines, nucleation of superconductivity and vortex patterns can be tuned in superconducting samples by varying their size and geometry [1]. The effects of the sample size, geometry and topology on the flux and condensate confinement have been very intensively studied during the last decade [2–8]. Single nanoplaquettes (discs, squares, triangles, loops, etc.) [9–15] their clusters [16–18] and huge arrays [19–21] were investigated.

[a] e-mail: mathieu.morelle@fys.kuleuven.ac.be

As it is clearly seen from the cited references, several Spanish groups have been actively working in this field, which nicely fits the main idea behind this special issue. In our manuscript we present the data on the crossover between the square and the rectangular geometry of individual plaquettes and on hybrid superconductor/ferromagnet structures. We have studied the effects of the sample size and geometry on vortex patterns and nucleation of superconductivity in these systems.

2 Rectangles

2.1 Theory

The nucleation of superconductivity is described by the linearized Ginzburg-Landau (LGL) equation [22]:

$$\frac{1}{2m^\star}\left(\frac{\hbar\nabla}{i} - 2e\boldsymbol{A}\right)\Psi = -\alpha\Psi\,, \tag{1}$$

where $\boldsymbol{A}$ is the vector potential corresponding to the applied magnetic field. Together with the superconductor/vacuum boundary condition [23]:

$$\left(\frac{\hbar\nabla}{i} - 2e\boldsymbol{A}\right)\Psi\Big|_n = 0\,, \tag{2}$$

where the subscript n means the normal component at the boundary line, the problem is then fully defined.

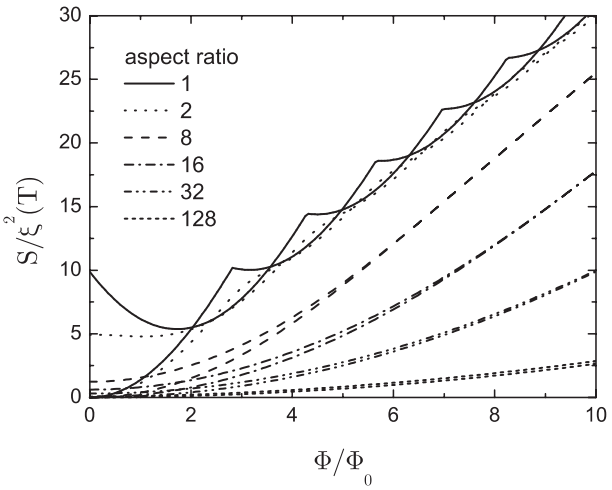

Fig. 1. Lowest two eigenvalues of the LGL equation for the mesoscopic rectangle for different aspect ratios, as a function of magnetic flux Φ/Φ_0, with superconductor-vacuum boundary conditions. The flux is defined as $\Phi = \mu_0 HS$, with S the surface of the rectangle, $\mu_0 H$ the applied magnetic field and $\Phi_0 = h/2e$ the superconducting flux quantum. Along the vertical axis the critical temperature T_c is linearly decreasing with increasing $S/\xi^2(T)$.

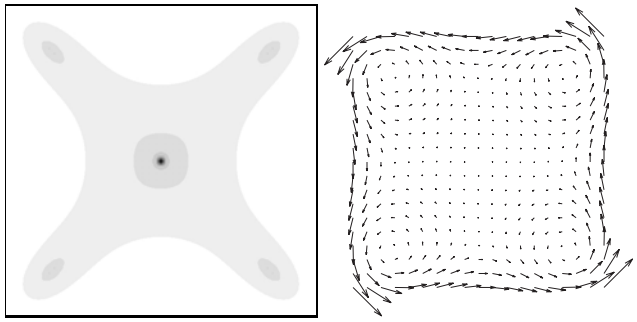

Fig. 2. The square is shown for a field of $5.5\Phi/\Phi_0$. The figure at the left shows the density of the order parameter $|\Psi|^2$. Dark regions indicate a low density of the order parameter $|\Psi|$. The figure at the right shows the super currents. The vorticity at this field is three and is generated by four vortices on the diagonals and one antivortex in the center. Both figures are a zoom of the central region of the structure. The square has a side that is 1/16 of the full square.

However, solving these equations for arbitrary geometries poses a considerable problem, due to the presence of the vector potential in equation (2). Nevertheless we have been able to simplify the problem significantly by introducing a vector potential gauge for regular polygons [24] with a zero normal component to the boundary line. Subsequently the boundary condition reduces to the Neumann boundary condition:

$$\nabla\Psi|_n = 0\,. \tag{3}$$

This choice of vector potential together with a basis set obeying the Neumann boundary conditions, allows us to redefine the problem as an eigenvalue problem. For the basis set we have taken the eigenfunctions of the zero field problem. Moreover, due to the rotational symmetry of the considered problems, the solutions of the LGL equation (1) can be characterized by the irreducible representations (irreps) of the corresponding symmetry group. For instance, in the case of a rectangle, which has a C_2 symmetry, the group contains two irreps A and B [25,15].

The solutions corresponding to irrep A and B have respectively no vortex, and one vortex in the center of the rectangle. However an exception is formed by the square which is a rectangle with aspect ratio $\zeta = 1$. Consequently the appropriate symmetry group is C_4. We then have solutions corresponding to irreps A, B, E_+ and E_- which have respectively no vortex, a giant $2\Phi_0$-vortex, a vortex and an antivortex in the center of the square [11]. Besides the central vortex we only observe vortices in the square on the diagonals and on the axes close to the center at the $T_c(H)$ phase boundary, which is the lowest eigenvalue of the LGL equation (1). Since the LGL equation is a linear equation, it is necessary that the solutions for a square have the same C_4 symmetry as the given problem. Therefore vortices on the diagonals and axes are always present in quartets as for example in Figure 2. Consequently the total vorticity of a state, which is given by the sum of the vorticity of the different vortices, can only change by a multiple of four within one irrep.

It is quite surprising that at certain values of magnetic field we find a solution with an antivortex in the center of the square, since an antivortex carries a flux quantum Φ_0 with the opposite orientation of the applied flux. Nonetheless the spontaneous generation of a quartet of vortices and an antivortex in the center is preferred above the generation of a giant $3\Phi_0$-vortex in the center. This can be understood from the symmetry requirements and the fact that giant vortices in bulk material carry an energy proportional to the square of the number of flux quanta. However, we observe that the area of the vortex-antivortex pattern is very small (see Fig. 2) at the $T_c(H)$ phase boundary, this means that the vortices and antivortex form an ensemble carrying three Φ_0.

Increasing the aspect ratio from one removes the antivortex from the center and replaces it by an ensemble of a vortex in the center and two antivortices next to it at a close distance. Moreover at aspect ratio $\zeta = 1.02$ no antivortices can be observed in the rectangle anymore. In addition vortices can be found in the rectangle on the longest axis and on the bisectors of the corners at the $T_c(H)$ phase boundary (see Fig. 3).

When examining the $T_c(H)$ phase boundary more closely, we observe that the $T_c(H)$ phase boundary is constructed out of a repeating sequence of branches belonging to the different irreps. Starting from zero at zero magnetic field, the vorticity increases with one at every cusp where the lowest solution of the LGL equation switches between branches belonging to different irreps. However, we notice with increasing aspect ratio ζ that the oscillations at the $T_c(H)$ phase boundary become smaller, until they become unnoticeable. Additionally the slope of the $T_c(H)$ phase boundary is lowered with increasing aspect ratio.

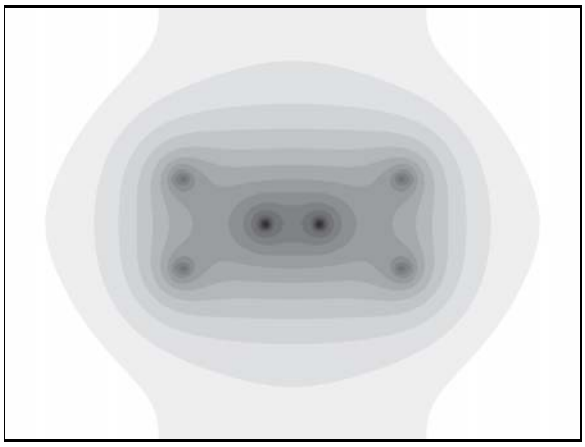

Fig. 3. The figure shows the density of the order parameter $|\Psi|^2$ in a rectangle with aspect ratio 4/3 and a magnetic field corresponding to $9.5\Phi/\Phi_0$. Dark regions indicate a low density of the order parameter $|\Psi|^2$. A pair of vortices is located symmetrically on the long axis and a quartet is positioned on the bisectors of the four corners.

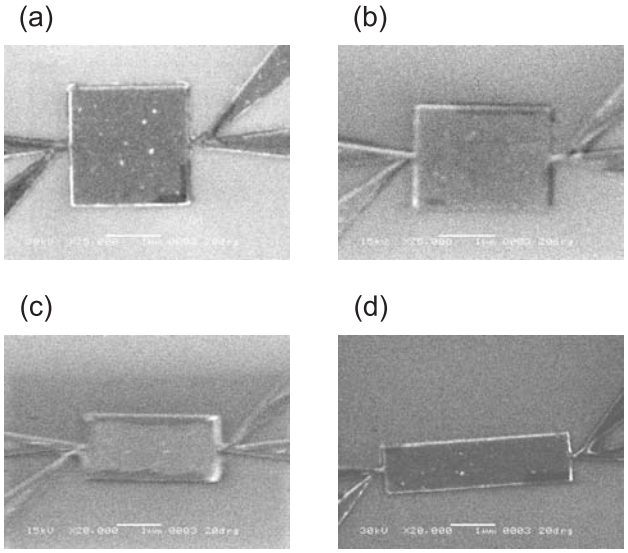

Fig. 4. SEM micrograph (a) of a Al square with lateral dimensions 2×2 μm^2 (ζ=1) and of a rectangle with lateral dimensions of (b) 1.73×2.31 μm^2 (ζ=4/3), (c) 1.41×2.83 μm^2 (ζ=2) and (d) 1×4 μm^2 (ζ=4).

Eventually the phase boundary evolves into a parabolic field dependence for the largest aspect ratios, analogous to the solution for a line [15].

Following the evolution of the vortex patterns in the rectangle within one irrep and not along the $T_c(H)$ phase boundary, which always corresponds to the lowest eigenvalue, we observe that the vortices enter by two through the middle of the longest sides, and naturally by four in the case of the square. Then they move towards the center with increasing field, where they form a giant vortex together with the vortex already present in the center depending on the irrep. In the case of the square the giant vortex then splits again with increasing field and the individual vortices move along the diagonals. In the case of the rectangle the giant vortex also splits into individual vortices, whereafter they first move along the long axis with increasing field. Eventually two pairs of vortices will melt at the two cross points of the bisectors with the long axis. After that they split again and move along the bisectors towards the corners of the rectangle.

With increasing magnetic field more and more vortices will be positioned on the bisectors at the $T_c(H)$ phase boundary. These vortices will be pushed towards the corners of the rectangle, however the vortices can not come too close to the corners since the order parameter $|\Psi|^2$ is higher at the corners, as expected from the studies of nucleation of superconductivity at wedges [26–31]. We also note that the magnetic field at which vortices will start to position themselves on the bisectors rises fast with increasing aspect ratio. So at the $T_c(H)$ phase boundary the vortex patterns for the larger aspect ratios will be predominantly one dimensional.

2.2 Sample characteristics

To investigate experimentally the crossover square-rectangle, four rectangles with different aspect ratio (ζ=1,4/3, 2 and 4) were studied in this paper. They were all evaporated in the same run. The four structures have the same area of $S = 4$ μm^2. A SEM micrograph of the studied samples is shown in Figure 4. The rectangles with aspect ratio ζ=1, 4/3, 2 and 4 have dimensions of 2×2 μm^2, 1.73×2.31 μm^2, 1.41×2.83 μm^2 and 1×4 μm^2. The thickness τ is 39 nm and the coherence length of the co-evaporated reference sample is 156 nm.

The samples were prepared by thermal evaporation of Al on a SiO_2 substrate. The patterns are defined by electron beam lithography before the evaporation of the Al film. After the deposition, the desired structures are obtained with a lift-off procedure. Wedge shaped current and voltage leads with an opening angle of $\Gamma = 15°$ and with a narrow width of the interface between the rectangles and the current leads were used in order to minimize their influence on the superconducting properties of the rectangles [14,32]. The $T_c(H)$ phase boundary is measured by four-point resistance measurements using a lock-in amplifier. An ac transport current of 0.1 μA is sent through the two current leads (horizontal contacts in Fig. 4). In order to construct the $H-T$ phase diagram a set of $R(H)$ magnetoresistance curves are measured at various temperatures. The phase line is in a next step extracted from the data using a certain resistance criterion R_c.

2.3 Resistive transitions

The resistive transitions of the mesoscopic rectangles with different aspect ratio are presented in Figure 5 for different magnetic fields. The square and the two rectangles with the smallest elongation show a resistive transition composed of two distinct parts: a broad transition at high

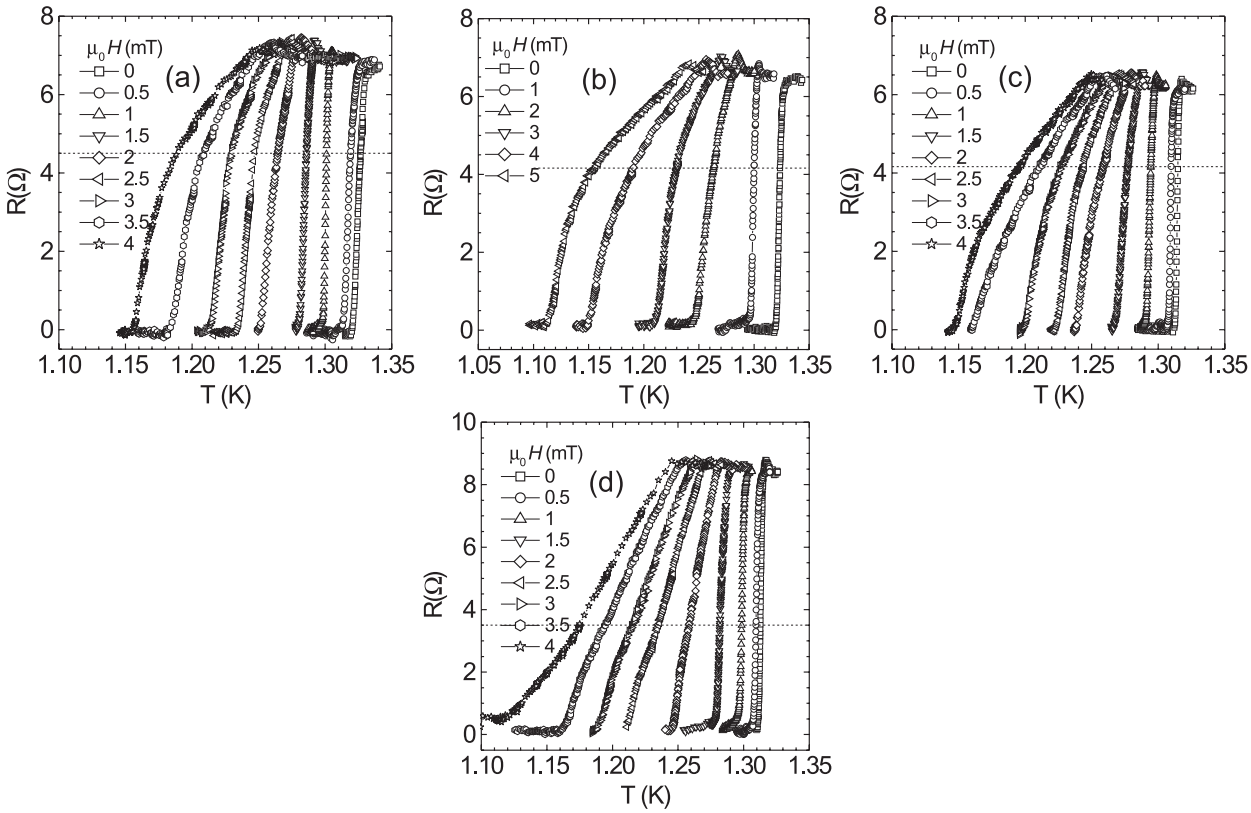

Fig. 5. Resistive transitions $R(T)$ for (a) a square ($\zeta = 1$) and a rectangle with (b) $\zeta = 4/3$, (c) $\zeta = 2$ and (d) $\zeta = 4$ in different magnetic fields. The dashed lines show the resistance criteria used to determine the $T_c(H)$ phase boundaries.

temperatures followed by a sharp drop. This is very similar to previous experimental results on a mesoscopic triangle [14]. It was shown that the two different regimes are arising from the difference in critical field of the contact leads and of the structure. The nucleation of superconductivity occurs first in the wedge shaped contacts and is then followed by the nucleation in the rectangle itself.

Small resistance anomalies, characterized by an overshoot resistance above the value of the resistance in the normal state R_n, are seen. They are created by the presence of a superconducting/normal interface around the voltage contacts due to the difference of critical temperature in the different parts of the sample [14].

Figure 5d shows the resistance transition of a mesoscopic rectangle with $\zeta = 4$. The rectangle with the smallest aspect ratio exhibits a different temperature dependence of the resistance compared to the other rectangles and to the triangle with the same current and voltage contacts presented in reference [14]. No sharp transition in the lower part of the $R(T)$ curve is observed except for the curve at 3.5 mT where a sharper transition can be seen starting at approximately 3 Ω. However, this effect is much weaker than in the previous samples. Contrary to the curve at 3.5 mT, the one measured at 4 mT shows the opposite behavior. Below ∼3 Ω, the transition broadens. The reason for this deviating behavior is more easily understood from the $H-T$ phase diagram and will therefore be discussed further down.

2.4 Phase boundary

To extract the phase boundary of the square from the measured data, the resistance criterion of 2/3 R_n is used, corresponding to the value where the slope of the resistance curves starts to change. The constructed $H-T$ diagram is displayed in Figure 6 and is compared with theoretical calculations (full line in Fig. 6). While previous transport measurements on a mesoscopic square [1,16] showed a strongly oscillating $T_c(H)$ dependence superimposed with a pronounced quadratic background, our results are in very good agreement with the theoretical predictions. Only a smaller coherence length $\xi(0)$=135 nm was used. The second parameter S used to compare the experimental and the theoretical data was found to be within the error margin of the determined area from SEM and AFM measurements. The main difference between the presented experimental phase boundary and previous reports is the shape and the size of the current and voltage contacts that can be extremely invasive in mesoscopic superconductors.

The experimental $T_c(H)$ curve of the different rectangles is presented in Figures 7, 8 and 9. The critical temperature of the rectangles with ζ=4/3 (Fig. 7) and 2 (Fig. 8) shows small oscillations superimposed with a linear dependence of the magnetic field. They have an almost identical phase boundary as the square (see Fig. 6). Only very small changes in the position of the cusps are observed.

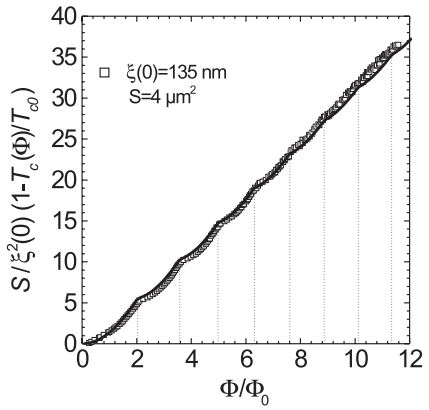

Fig. 6. Experimental $T_c(H)$ phase boundary of a square. The open squares represent the measured value using the measured sample size $S = 4\ \mu\text{m}^2$ and the coherence length $\xi(0) = 135$ nm. The full line is the theoretical curve (see Fig. 1).

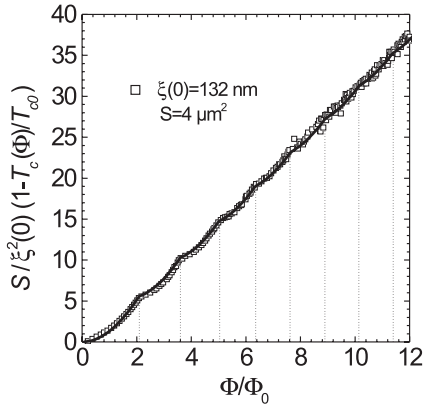

Fig. 7. Experimental $T_c(H)$ phase boundary of a rectangle with $\zeta = 4/3$. The open squares represent the measured value using the measured sample size $S = 4\ \mu\text{m}^2$ and the coherence length $\xi(0) = 132$ nm. The full line is the theoretical curve (see Fig. 1).

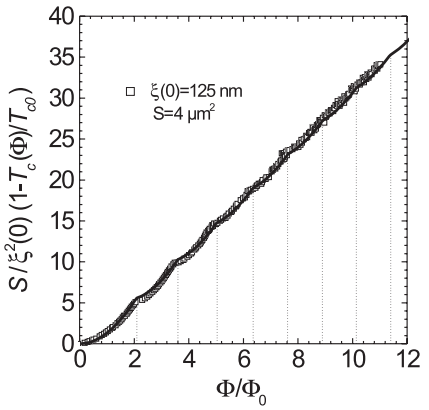

Fig. 8. Experimental $T_c(H)$ phase boundary of a rectangle with $\zeta = 2$. The open squares represent the measured value using the measured sample size $S = 4\ \mu\text{m}^2$ and the coherence length $\xi(0) = 125$ nm. The full line is the theoretical curve (see Fig. 1).

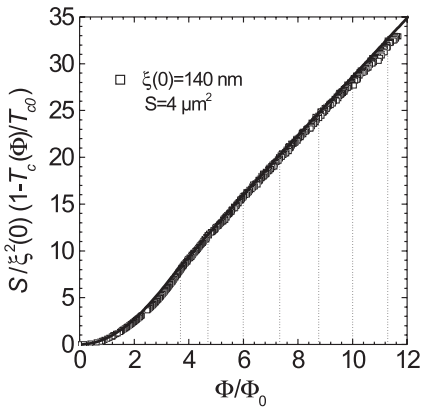

Fig. 9. Experimental $T_c(H)$ phase boundary of a rectangle with $\zeta = 4$. The open squares represent the measured value using the measured sample size $S = 4\ \mu\text{m}^2$ and the coherence length $\xi(0) = 140$ nm for a resistance criterion of 40% of R_n. The full line is the theoretical curve (see Fig. 1).

The magnetic field value where the vorticity changes from L to $L + 1$ is slightly delayed when changing the value of ζ from one. No significant change in the slope and the amplitude of the oscillations could be observed.

A very good agreement between the experimental and the theoretical curves, as well as for the position of the cusp as for the amplitude of the oscillations, is obtained for these two rectangles. Even a large deformation of the square ($\zeta = 2$) gives negligible changes in the phase boundary. It seems that *the angle of the corners and the area S play the most important roles in the determination of the phase boundary*. It was shown theoretically that already a small change in the aspect ratio would change the vortex configuration at the nucleation of superconductivity. These different vortex arrangements however do not affect substantially the lowest Landau levels.

For a rectangle with aspect ratio $\zeta = 4$, the phase boundary (Fig. 9) is strongly transformed compared to the case of the square. The oscillations are hardly seen and the position of the first vortex entry is delayed to $\Phi/\Phi_0 \cong 3.7$ (left dotted line in Fig. 9) instead of the value of $\Phi/\Phi_0 \cong 2$ found for a square. A good agreement between the experimental and the theoretical curves is obtained for a resistance criterion of 40% of R_n.

Increasing further the elongation will lead to a delay of the entry of the first vortex in the sample so that the phase boundary will display a parabolic dependence on the field as long as the first vortex is not entering the sample. For an infinitely long rectangle with finite width, the case of a thin wire or film is recovered.

3 Hybrid structures

3.1 Introduction

Hybrid superconductor/ferromagnet structures have recently attracted a considerable attention. The interplay of superconductivity and magnetism has mainly been studied on superconducting thin films with arrays of magnetic

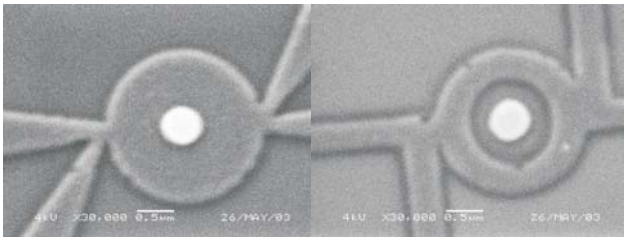

Fig. 10. Scanning electron micrographs of the disk and loop with magnetic dots.

dots [20,21,33], with the emphasis on the pinning properties of these structures.

We have investigated the nucleation of superconductivity in individual superconducting structures with a single perpendicularly magnetized magnetic dot. A superconducting disk with a magnetic dot on the top and a superconducting loop enclosing a dot were studied. The dot is separated from the superconducting disk by an insulating spacer layer in order to avert proximity effects and ensure that the interaction between superconductivity and magnetism in both samples has purely *magnetic* character [34].

The superconducting $T_c(H)$ phase boundaries were obtained by transport measurements, applying the magnetic field perpendicularly to the surface of the samples. Both $T_c(H)$ phase boundaries are asymmetric with respect to the polarity of the applied magnetic field, with the maximum critical temperatures attained for the finite values of the external field. However, even though the sizes and magnetization of dots were identical in both samples, the maximum critical temperature of the disk has been observed for an applied magnetic field parallel to the magnetization of the dot (hereafter positive applied fields), whereas the loop exhibits the maximum critical temperature for an applied magnetic field antiparallel to the magnetization of the dot (hereafter negative applied fields).

3.2 Sample fabrication and properties

The samples were fabricated on SiO_2 substrates by electron beam lithography and lift-off technique. The preparation of the samples involved three subsequent phases, in which the contacts and alignment markers, superconducting structures and magnetic dots, respectively, were patterned and thermally grown. For the details of the fabrication procedure, please refer to [35] The thickness of Al superconducting disk and loop is 60 nm, the radius of the disk is 1.08 μm, whereas the inner and outer radii of the loop are 0.55 μm and 1.05 μm, respectively. Scanning electron micrographs of the samples are shown in Figure 10.

The dots with the radius of 0.27 μm consist of 10 bilayers of Co and Pd with the individual thicknesses of 0.4 nm and 1 nm, respectively, on 2.5 nm Pd buffer layer. This multilayer is know to provide a complete remanence and nearly perfect squareness of the hysteresis loop [33,36]. Figure 11 shows the room temperature hysteresis loop of the co-evaporated Co/Pd reference film obtained by the

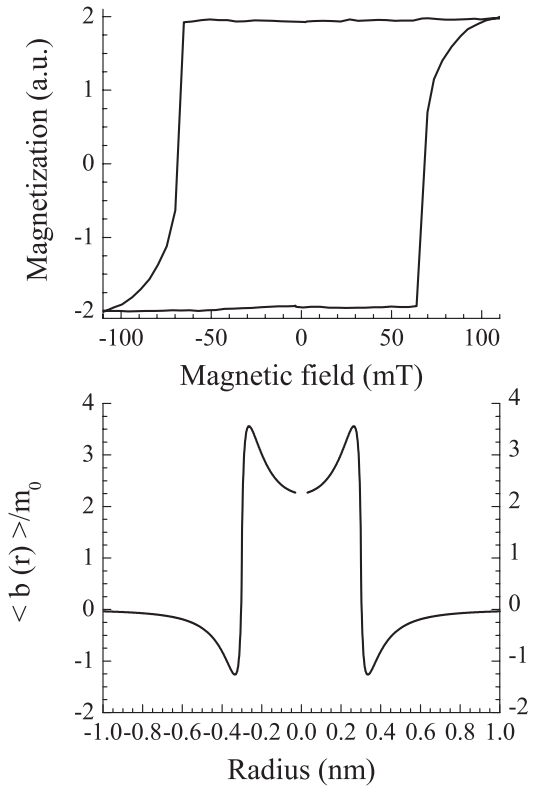

Fig. 11. Hysteresis loop of the co-evaporated Co/Pd reference film and the spatial profile of the stray field generated by the magnetic dot, obtained by magnetostatic calculations.

MOKE measurements (upper figure) and the calculated spatial profile of the stray field (lower figure). Prior to the measurements, the dots were saturated in the magnetic field of 500 mT. As the externally applied field did not exceed 30 mT, the magnetization of the dots remained unaffected during the experiment.

3.3 Results

The onset of superconductivity in the structure was studied by measuring the superconducting $T_c(H)$ phase boundary. The phase boundary was found resistively, from four-point transport measurements, in a cryogenic setup at temperatures down to 1.11 K, with the temperature and field resolution of 0.5 mK and 5 μT, respectively. The transport current with the effective value of 100 nA and frequency 27.7 Hz was used, whilst the signal-to-noise ratio was being improved by a lock-in amplifier.

Figure 12 displays resistive transitions of the disk which are strongly asymmetric with respect to the polarity of an applied field. The mean field transition temperature, defined conventionally as the temperature at which the resistance is $R_n/2$, in the applied magnetic field of +2 mT is equal to the transition temperature in −1 mT. This feature of the resistive transitions is reproduced for higher fields, as well. More importantly, the critical temperature in zero applied field is not the maximum critical temperature of the structure. The structure attains the maximum

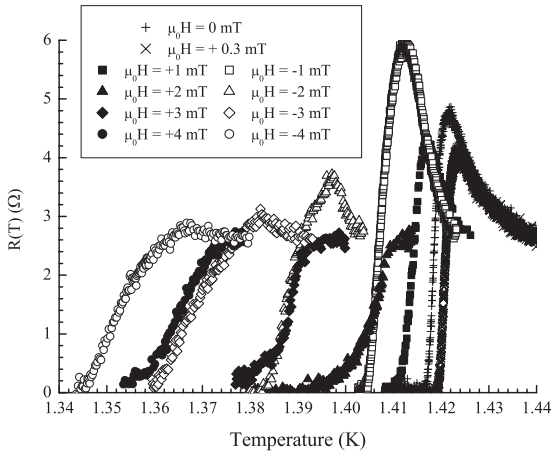

Fig. 12. $R(T)$ transition in a constant applied magnetic field. Filled symbols indicate transitions in the positive applied fields, whereas open symbols present transition in the negative magnetic fields.

critical temperature when exposed to the magnetic field of +0.3 mT. The difference between the maximum critical temperature T_{cm} and zero-field critical temperature T_{c0} is approximately 2.5 mK.

Figure 13 shows the $T_c(H)$ phase boundaries of the disk (upper figure) and the loop (lower figure). Dotted curves are experimentally obtained phase boundaries, solid lines present theoretical fits, whereas the dashed line in the upper figure shows the theoretical phase boundary of the disk without the dot.

The superconducting phase boundaries exhibit a pronounced field-polarity dependence. The maximum critical temperatures are attained for finite values of the applied magnetic field. The direction of the shift of $T_c(H)$ phase boundary near T_{c0}, for a fixed orientation of the magnetization m, depends upon the intensity of the stray field of the magnetic dot, that is, upon the intensity of m. The shift can come about as a result of the cancellation of the total flux generated by the magnetic dot, or due to a change in the kinetic energy of the superconducting condensate in the disk, accompanied by a switch in the vorticity by one. The former shifts the phase boundary in the direction opposite to the magnetization of the dot and the maximum critical temperature is observed for a finite *negative* applied field, whereas the latter provides that the maximum critical temperature is achieved for a finite applied field parallel to the magnetization of the dot, that is for a finite *positive* field. Which of these competing effects prevails depends strongly upon the intensity of magnetization of the magnetic dot, as well as upon the parameters of the superconducting structure.

The experimental data have been analyzed by using the GL theory. Given that the samples are thinner than the coherence length $\xi(T)$, as well as that boundaries of the samples impose the axial symmetry, it is possible to reduce the dimensionality of the problem to the 1D case in the vicinity of the phase boundary and express the dimensionless order parameter $\psi(r,\phi)$ using the cylindrical

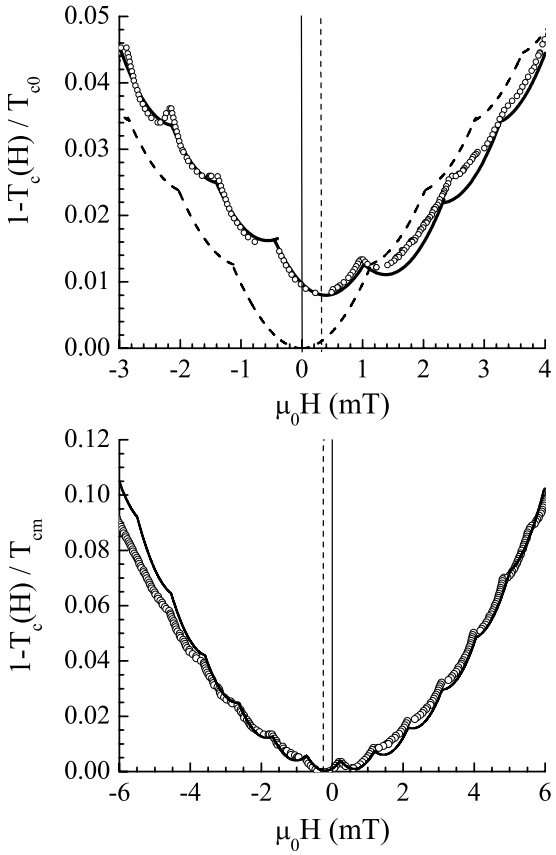

Fig. 13. $R(T)$ transition in a constant applied magnetic field. Filled symbols indicate transitions in the positive applied fields, whereas open symbols present transition in the negative magnetic fields.

coordinate system as

$$\psi(r,\phi) = f(r)\exp(-iL\phi)\ , \tag{4}$$

where $f(r)$ is the modulus of the order parameter, L stands for the winding number (vorticity). The superconducting $T_c(H)$ phase boundary of the loop has been obtained assuming that the modulus of the order parameter is constant, whereas for the disk the following the trial function for the modulus of the order parameter has been used,

$$f(r) = p_1 \cdot \exp\left(-q\frac{r^2}{R^2}\right)\cdot\left(\left(\frac{r}{R}\right)^L + p_2\left(\frac{r}{R}\right)^{L+1} + p_3\left(\frac{r}{R}\right)^{L+2} + p_4\left(\frac{r}{R}\right)^{L+3}\right), \tag{5}$$

where p_1, p_2, p_3 and p_4 are the variational parameters, R is the radius of the disk, whereas q is found from the vacuum boundary condition for the order parameter ($f'(R) = 0$)

$$q = \frac{L + p_2(L+1) + p_3(L+2) + p_4(L+3)}{2(1 + p_2 + p_3 + p_4)}. \tag{6}$$

Using equations (4) and (5) the GL energy is found as a function of the variational parameters [37]. The values

of the variational parameters are calculated by minimizing the GL energy. Comparing the energies of states with different L the superconducting $T_c(H)$ phase boundary of the disk is found. The magnetization of the dot m has been chosen to provide the best qualitative and quantitative agreement between the theory and the experiment in the vicinity of T_{c0}.

4 Conclusions

The superconducting/normal $T_c(H)$ phase boundary for samples of different geometries and for the superconductor/ferromagnet hybrids have been studied experimentally and theoretically. Rectangles with small deformation compared to the square give only minor difference in $H-T$ phase diagrams. Major differences are observed for strongly elongated rectangles where the crossover from a linear to a parabolic field dependence of the critical temperature could be seen.

We were able to find a good agreement between our experimental $T_c(H)$ data and the theoretical model, based on the linearized GL theory, for all studied samples.

It has been demonstrated that hybrid superconductor/ferromagnet structures have the $T_c(H)$ phase boundary which is shifted along the field axis. As a result, the maximum critical temperatures of the structures are attained for a finite value of the applied magnetic field. The direction of the shift in the $T_c(H)$ phase boundary is not caused by a simple compensation effect of the flux generated by the dot, but strongly depends on parameters of the dot and superconducting sample.

This work has been supported by the Belgian IUAP, the Flemish Research Council K.U.Leuven GOA/2004/02 and FWO-programmes, and by the ESF programme VORTEX. The authors would like to thank O. Popova for the X-rays measurements. G.T. is a postdoctoral fellow of the Research Council of the K.U.Leuven, M.M. is a postdoctoral fellow of IWT-Vlaanderen.

References

1. V.V. Moshchalkov, L. Gielen, C. Strunk, R. Jonckheere, X. Qiu, C. Van Haesendonck, Y. Bruynseraede, Nature **373**, 319 (1995)
2. J.G. Rodrigo, H. Suderow, S. Vieira, Phys. Stat. Sol. B **237**, 386 (2003)
3. H. Suderow, E. Bascones, A. Izquierdo, F. Guinea, S. Vieira, Phys. Rev. B **65**, 100519 (2002)
4. H. Suderow, A. Izquierdo, S. Vieira, Physica C **332**, 327 (2000)
5. M. Poza, E. Bascones, J.G. Rodrigo, N. Agrait, S. Vieira, F. Guinea, Phys. Rev. B **58**, 11173 (1998)
6. J.G. Rodrigo, N. Agrait, C. Sirvent, S. Vieira, Phys. Rev. B **50**, 12788 (1994)
7. J.J. Palacios, Physica B **256-258**, 610 (1998)
8. J.J. Palacios, Phys. Rev. B **58**, R5948 (1998)
9. J.J. Palacios, Phys. Rev. Lett. **84**, 1796 (2000)
10. J.J. Palacios, F.M. Peeters, B.J. Baelus, Phys. Rev. B **64**, 134514 (2001)
11. L.F. Chibotaru, A. Ceulemans, V. Bruyndoncx, V.V. Moshchalkov, Nature **408**, 833 (2000)
12. L.F. Chibotaru, A. Ceulemans, V. Bruyndoncx, V.V. Moshchalkov, Phys. Rev. Lett. **86**, 1323 (2001)
13. B.J. Baelus, F.M. Peeters, Phys. Rev. B **65**, 104515 (2002)
14. M. Morelle, Y. Bruynseraede, V.V. Moshchalkov, Phys. Stat. Sol. B **237**, 365 (2003)
15. G. Teniers, L.F. Chibotaru, A. Ceulemans, V.V. Moshchalkov, Europhys. Lett. **63**, 296 (2003)
16. V. Bruyndoncx, J.G. Rodrigo, T. Puig, L. Van Look, V.V. Moshchalkov, R. Jonckheere, Phys. Rev. B **60**, 4285 (1999)
17. T. Puig, E. Rosseel, L. Van Look, M.J. Van Bael, V.V. Moshchalkov, Y. Bruynseraede, R. Jonckheere, Phys. Rev. B **58**, 5744 (1998)
18. T. Puig, E. Rosseel, M. Baert, M.J. Van Bael, V.V. Moshchalkov, Y. Bruynseraede **70**, 3155 (1997)
19. M. Baert, V.V. Metlushko, R. Jonckheere, V.V. Moshchalkov, Y. Bruynseraede, Phys. Rev. Lett. **74**, 3269 (1995)
20. J.E. Villegas, E.M. Gonzalez, M.I. Montero, I.K. Schuller, J.L. Vicent, Phys. Rev. B **68**, 224504 (2003)
21. J.E. Villegas, S. Savel'ev, F. Nori, E.M. Gonzalez, J.V. Anguita, R. García, J.L. Vicent, Science **302**, 1188 (2003)
22. P.-G. de Gennes. *Superconductivity of Metals and Alloys* (Benjamin, New York, 1966)
23. D. Saint-James, P.-G. de Gennes. Phys. Lett. **7**, 306 (1963)
24. L.F. Chibotaru, A. Ceulemans, G. Teniers, V. Bruyndoncx, V.V. Moshchalkov, Eur. Phys. J. B **27**, 341 (2002)
25. L.D. Landau, E.M. Lifshitz, *Quantum Mechanics*, 2nd edn. (Pergamon, Oxford, 1975)
26. A. Houghton, F.B. McLean, Phys. Lett. **19**, 172 (1965)
27. A.P. van Gelder, Phys. Rev. Lett. **20**, 1435 (1968)
28. V.M. Fomin, J.T. Devreese, V.V. Moshchalkov, Europhys. Lett. **42**, 553 (1998)
29. F. Brosens, J.T. Devreese, V.M. Fomin, V.V. Moshchalkov, Solid State Comm. **111**, 565 (1999)
30. V.A. Schweigert, F.M. Peeters, Phys. Rev. B **60**, 3084 (1999)
31. S.N. Klimin, V.M. Fomin, J.T. Devreese, V.V. Moshchalkov, Solid State Comm. **111**, 589 (1999)
32. M. Morelle, G. Teniers, L.F. Chibotaru, A. Ceulemans, V.V. Moshchalkov, Physica C **369**, 351 (2002)
33. M. Lange, M.J. Van Bael, Y. Bruynseraede, V.V. Moshchalkov, Phys. Rev. Lett. **90**, 197006 (2003)
34. D. S. Golubović, W.V. Pogosov, M. Morelle, V.V. Moshchalkov, Appl. Phys. Lett. **83**, 8 (2003)
35. D.S. Golubović, W.V. Pogosov, M. Morelle, V.V. Moshchalkov, Phys. Rev. B **68**, 172503 (2003)
36. A.N. Grigorenko, S.J. Bending, M.J. Van Bael, M. Lange, V.V. Moshchalkov, H. Fangohr, P.A.J. de Groot, Phys. Rev. Lett. **90**, 237001 (2003)
37. W.V. Pogosov, Phys. Rev. B **65**, 224511 (2002)